AD-A064 882 VIRGINIA POLYTECHNIC INST AND STATE UNIV BLACKSBURG --ETC F/G 6/7
STUDIES OF LIMB-DISLODGING FORCES ACTING ON AN EJECTION SEAT OC--ETC(U)
JAN 79 D J SCHNECK AFOSR-77-3296
UNCLASSIFIED VPI-E-78-16 AMRL-TR-78-103 NL

| OF |
AD
A064882

END
DATE
FILMED
4-79
DDC

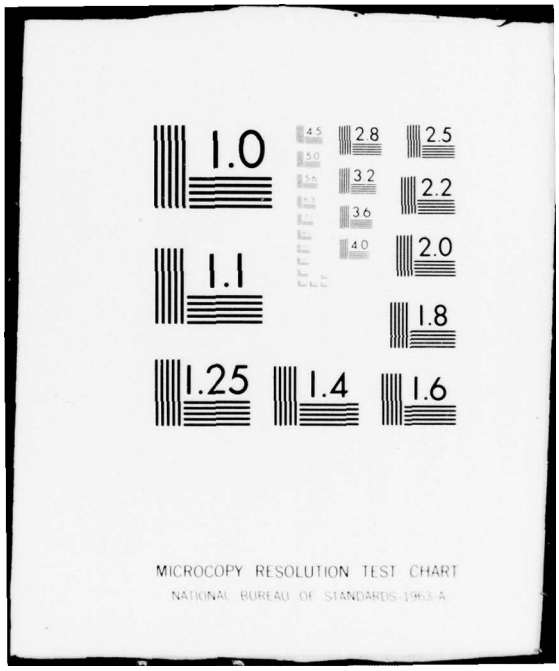
1.0
1.1
1.25
1.4
1.6
1.8
2.0
2.2
2.5
2.8
3.2
3.6
4.0
4.5
5.0
5.6
MICROCOPY RESOLUTION TEST CHART
NATIONAL BUREAU OF STANDARDS-1963-A

(2) NW LEVEL II

AMRL-TR-78-103

STUDIES OF LIMB-DISLODGING FORCES ACTING ON AN EJECTION SEAT OCCUPANT

DANIEL J. SCHNECK, PhD

VIRGINIA POLYTECHNIC INSTITUTE AND STATE UNIVERSITY
BLACKSBURG, VIRGINIA 24061

JANUARY 1979

Approved for public release distribution unlimited.

AEROSPACE MEDICAL RESEARCH LABORATORY
AEROSPACE MEDICAL DIVISION
AIR FORCE SYSTEMS COMMAND
WRIGHT-PATTERSON AIR FORCE BASE, OHIO 45433

NOTICES

When US Government drawings, specifications, or other data are used for any purpose other than a definitely related Government procurement operation, the Government thereby incurs no responsibility nor any obligation whatsoever, and the fact that the Government may have formulated, furnished, or in any way supplied the said drawings, specifications, or other data, is not to be regarded by implication or otherwise, as in any manner licensing the holder or any other person or corporation, or conveying any rights or permission to manufacture, use, or sell any patented invention that may in any way be related thereto.

Please do not request copies of this report from Aerospace Medical Research Laboratory. Additional copies may be purchased from:

National Technical Information Service
5285 Port Royal Road
Springfield, Virginia 22161

Federal Government agencies and their contractors registered with Defense Documentation Center should direct requests for copies of this report to:

Defense Documentation Center
Cameron Station
Alexandria, Virginia 22314

TECHNICAL REVIEW AND APPROVAL

AMRL-TR-78-103

This report has been reviewed by the Information Office (OI) and is releasable to the National Technical Information Service (NTIS). At NTIS, it will be available to the general public, including foreign nations.

This technical report has been reviewed and is approved for publication.

FOR THE COMMANDER

HENNING E. VON GIERKE
Director
Biodynamics and Bioengineering Division
Aerospace Medical Research Laboratory

AIR FORCE/56780/2 February 1979 — 150

SECURITY CLASSIFICATION OF THIS PAGE *(When Data Entered)*

REPORT DOCUMENTATION PAGE

READ INSTRUCTIONS BEFORE COMPLETING FORM

1. REPORT NUMBER: AMRL-TR-78-103	2. GOVT ACCESSION NO.
3. RECIPIENT'S CATALOG NUMBER	
4. TITLE *(and Subtitle)*: STUDIES OF LIMB-DISLODGING FORCES ACTING ON AN EJECTION SEAT OCCUPANT.	5. TYPE OF REPORT & PERIOD COVERED: Final Report. 1 Mar 77 - 28 Feb 78
	6. PERFORMING ORG. REPORT NUMBER: VPI-E-78-16
7. AUTHOR(s): Daniel J. Schneck, PhD	8. CONTRACT OR GRANT NUMBER(s): AFOSR Grant Number 77-3296
9. PERFORMING ORGANIZATION NAME AND ADDRESS: Virginia Polytechnic Institute and State Univ. Department of Engineering Science and Mechanics Blacksburg, Virginia 24061	10. PROGRAM ELEMENT, PROJECT, TASK AREA & WORK UNIT NUMBERS: 61102F, 2312-V3-11
11. CONTROLLING OFFICE NAME AND ADDRESS: Aerospace Medical Research Laboratory, Aerospace Medical Division, Air Force Systems Command, Wright-Patterson Air Force Base, Ohio 45433	12. REPORT DATE: January 1979 13. NUMBER OF PAGES: 37
14. MONITORING AGENCY NAME & ADDRESS *(if different from Controlling Office)*: AFOSR-77-3296	15. SECURITY CLASS. *(of this report)*: Unclassified 15a. DECLASSIFICATION/DOWNGRADING SCHEDULE: N/A

16. DISTRIBUTION STATEMENT *(of this Report)*

41 P

Approved for public release; distribution unlimited

DDC RECEIVED FEB 26 1979 B

17. DISTRIBUTION STATEMENT *(of the abstract entered in Block 20, if different from Report)*

18. SUPPLEMENTARY NOTES

19. KEY WORDS *(Continue on reverse side if necessary and identify by block number)*

Biological and Medical Sciences	Windblast Injuries
Biodynamic Modeling	Flail Injury
Aerodynamic Forces	High-Speed Ejection
Inviscid Flow Theory	Potential Flow Theory
Human Body Model	Flow Separation

20. ABSTRACT *(Continue on reverse side if necessary and identify by block number)*

In this report, the forces tending to dislodge the limbs of an ejection seat occupant from one another, or from a restraining surface, are calculated in the absence of flow separation. For a simulated ejection taking place at an altitude of 10,000 feet, the results show that, based on published data for a pilot's average grip retention capability, the probability of his letting go is 100% if the ejection occurs at Mach numbers exceeding 0.72. Moreover, the probability of major flail injury is around 100% if the ejection Mach number exceeds around 1.25. One major factor which contributes to these large limb-

(over)

DD FORM 1 JAN 73 1473 EDITION OF 1 NOV 65 IS OBSOLETE

SECURITY CLASSIFICATION OF THIS PAGE *(When Data Entered)*

404 722

cont

Block 20. Abstract (cont'd.)

dislodging forces is the generation of stagnation points in the flow. In order to examine further the role played by flow separation around the blunt body segments, a complex velocity potential is developed to describe a stationary vortex pair located in the wake region of the flow. It remains to super-impose this vortex pair on the unseparated cross flow in order to ascertain the drag forces which contribute to limb dislodgement.

A

PREFACE

The work described herein was accomplished with the financial support of the Air Force Office of Scientific Research under grant number 77-3296. This was a mini-grant program follow-up to the author's participation in the 1976 USAF/ASEE Summer Faculty Fellowship Research Program, which was held at the Aerospace Medical Research Laboratory (AMRL) at Wright-Patterson Air Force Base, Ohio.

The author wishes to express his gratitude and appreciation to Dr. P. F. Iampietro, Director of Life Sciences, and Lt Col D. E. England, Program Manager (Mini-Grant Program), of AFOSR; and Dr. Henning E. von Gierke, Director of the Biodynamics and Bioengineering Division, Dr. Hans L. Oestreicher, Chief of the Mathematics and Analysis Branch, and Mr. Ints Kaleps, Research Scientist, of AMRL for their support, encouragement and review of this material.

SUMMARY

Problem

Statistical data show that windblast forces increase with aircraft speed to the point where an overall five or ten percent limb-flail injury rate rises to 40 percent or more. This is far from negligible, but control of the forces that produce excessive motion of the limbs of an ejection seat occupant can only be achieved if we increase our understanding of the aerodynamic loading to which a pilot is exposed during high-speed ejections. Toward this end, a mathematical model is being developed which is expected to provide aerodynamic data that can be used as input information to the Aerospace Medical Research Laboratory's Articulated Total Body Model. The latter can then be used to assess the kinematics of limb motion under the action of specific aerodynamic forces. In this report, the forces tending to dislodge the limbs of an ejection seat occupant from one another, or from a restraining surface, are calculated in the absence of flow separation. The results are then modified to show how the more realistic physical effects of separation of flow around the blunt body segments may be taken into consideration.

Approach

Limb-dislodging forces in the absence of flow separation are computed by integrating the pressure coefficient which was derived in an earlier report for the cross-flow over a limb-to-limb or limb-to-restraining surface contact configuration. Modifications to include the effects of separation of flow are then introduced by describing a distribution of inviscid vortices which originate from the separation of shear layers, and which can be superimposed on the unseparated potential flow solutions obtained thus far.

Results

For a simulated ejection taking place at an altitude of 10,000 feet, the results show that, based on published data for a pilot's average grip retention capability, the probability of his letting go is 100% if the ejection occurs at Mach numbers in excess of 0.72. That is, the aerodynamic forces are such that the pilot's musculo-skeletal system is not likely to withstand the tendency for dislodgement from a restraining surface if he is ejecting at Mach numbers exceeding 0.72. Moreover, the probability of major flail injury is around 100% if the ejection Mach number exceeds 1.25. One major factor which contributes to these large limb-dislodging forces appears to be the generation of stagnation points in the flow. In order to examine further the role played by flow separation around the blunt body segments, a complex velocity potential is developed to describe a stationary vortex pair located in the wake region of the flow. It remains to superimpose this vortex pair on the unseparated cross flow in order to ascertain the drag forces which contribute to limb dislodgement.

Conclusions

To the level of approximation in this report, one would have to conclude that the generation of stagnation points in the flow produces forces that can cause limb-dislodgement (with subsequent flail and possible serious injury). Moreover, these forces are sensitive to the angle at which the limb intercepts the flow, such that the higher the angle, the greater the tendency for dislodgement. And finally, the forces increase rapidly with speed of ejection, which correlates well with the finding that windblast injuries increase dramatically as a function of airspeed.

Recommendations

It is desirable to examine the time-course of the limb dislodging forces after the onset of windblast. That is, the forces computed in this report exist at the onset of ejection and are peak forces that prevail so long as the limb is in contact with a restraining surface. Once contact with the surface is broken, there follows a redistribution of forces, and this information is desirable input to the ATB simulation which provides kinematic data. The added complications resulting from separation of the flow and limb interactions need also to be further elucidated in an effort to define design criteria for safer ejections. There is interest in extending the analysis to include the head/neck configuration in order to shed some light on the factors that contribute to an oscillatory fore-aft head vibration. And finally, the effects of surface roughness (which may be due, in part, to the type of clothing being worn by the pilot), and compressibility effects of the flow (such as shock waves) should be assessed as to their first or second order influences on the factors that contribute to windblast injuries.

TABLE OF CONTENTS

LIST OF ILLUSTRATIONS

SECTION I

INTRODUCTON

Statistical data accumulated from five nations has brought to light the devastating effects of high-speed ejections from aircraft (Glaister, 1975). That is, the data show that windblast forces increase with aircraft speed to the point where an otherwise 5-10 percent limb-flail injury rate rises to 40 percent or more. This is far from negligible, but control of the forces that produce excessive motion of the limbs of an ejection seat occupant can only be achieved if we increase our understanding of the aerodynamic loading to which a pilot is exposed during high-speed ejections. In a recent report (Schneck, 1976) it was shown that it is feasible to formulate a mathematical model which can predict such aerodynamic loading. Results from this model can then be incorporated into the Aerospace Medical Research Laboratory's modified Calspan Model of the Articulated Total Body (ATB) in order to assess the kinematics of limb motion under the action of specified aerodynamic forces. In the earlier report, potential flow solutions were presented for estimating the pressure distribution around the forearm of a human body subjected to windblast. The work which follows expands these preliminary results, and extends them to include some effects of flow separation.

The body model used here for the analysis of windblast forces is represented again by the 15-linkage system of spherical, circular-cylindrical, truncated-conical and flat-plate segments shown in Figure 1 (see Schneck, 1976, for a complete description). Moreover, specific attention is focussed on the events which take place where a body segment is either in contact with a restraining surface, such as the forearm in contact with an arm rest, or, equivalently, where two body segments are in contact with one another, such as the upper arm pressing against the thorax. For this situation, the complex velocity potential for the aerodynamic cross-flow over the limbs (in the absence of flow separation) has been shown to be given by:

$$w = \pi a V \coth \frac{a\pi}{\chi}, \qquad (1)$$

which corresponds to the cross-flow streamline pattern depicted in Figure 2 for the cross-sectional geometric configuration shown, with $\chi = y + iz$ and $w = \Phi + i\Psi$. The streamlines illustrated are non-dimensionalized with respect to V and a.

In the section which follows, the forces tending to dislodge the limbs from one another, or from a restraining surface, are calculated in the absence of flow separation, i.e., for the situation depicted in Figure 2. In subsequent sections, the results are then modified to allow for the inclusion of the more realistic physical effects of separation of flow around the blunt body segments.

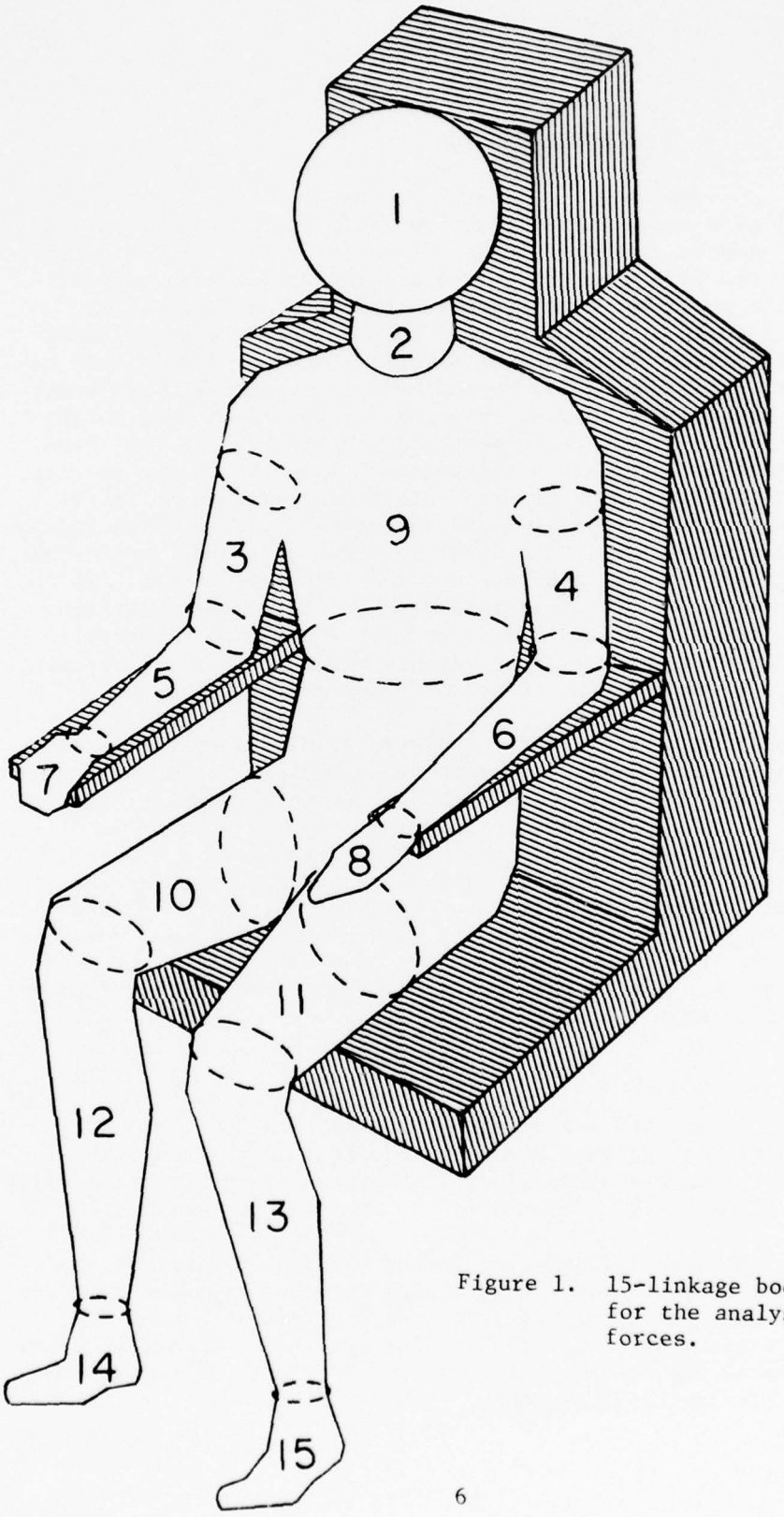

Figure 1. 15-linkage body model used for the analysis of windblast forces.

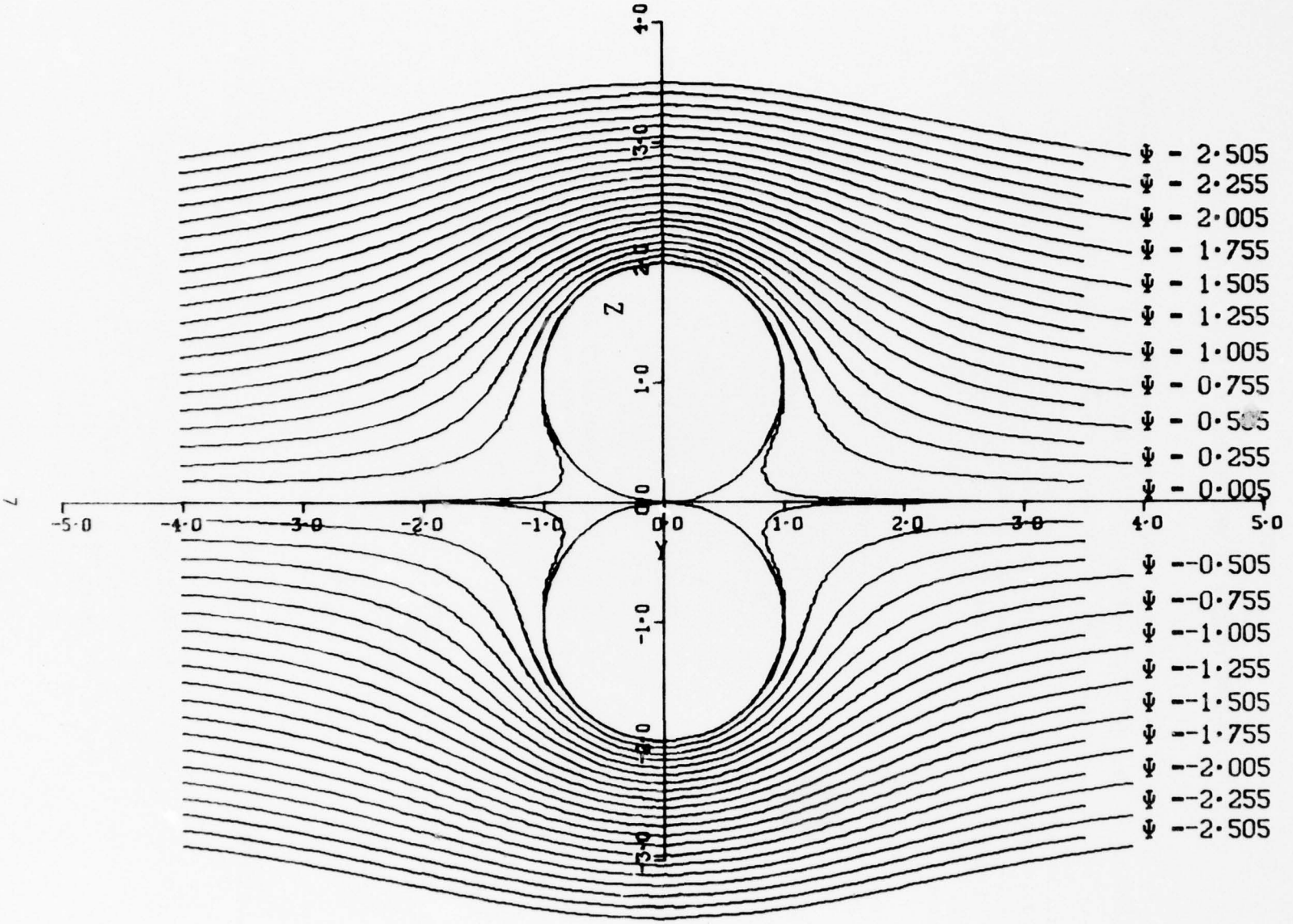

Figure 2. Cross-Flow streamline pattern for two circular-cylindrical body segments in line contact with one another.

SECTION II

LIMB DISLODGING FORCES IN THE ABSENCE OF FLOW SEPARATION

Let p designate the aerodynamic pressure existing at a point along the cylindrical surfaces illustrated in Figures 2 and 3. If γ defines the azimuthal coordinate such that $\tan \gamma = \frac{z-a}{y}$ (non-dimensionalized radius a = 1 in Figure 2), then the differential surface element $a(d\gamma)$ having unit length along the axis of the limb has a force on it of magnitude $df = p(a)(d\gamma)$ directed radially inward (see Figure 3). The component of this force tending to push the cylinders together (or pull them apart) is thus given by $df_z = -(p \sin \gamma)(a\, d\gamma)$, so that the net vertical force becomes:

$$f_z = \int_{-\pi/2}^{3\pi/2} -ap \sin \gamma \, d\gamma \text{ per unit length.} \tag{2}$$

Now, the pressure, p, was obtained earlier (Schneck, 1976) in the form of a pressure coefficient which, for the cylindrical configuration illustrated in Figure 2, is given by:

$$C_p = \frac{p - p_o}{\frac{1}{2}\rho U_o^2} = \sin^2 \alpha \left[1 - \frac{a^2\pi^4}{4z^2} \operatorname{sech}^4 \frac{\pi y}{2z}\right] \tag{3}$$

Before substituting equation (3) into equation (2) and performing the indicated integration, it is convenient to make some transformations and redefine certain variables. Referring to Figure 3, we note that the equation of the circle is $r^2 = 2az$, while $r = 2a \sin \theta$ and $y = r \cos \theta$. Thus,

$$\frac{\pi y}{2z} = \frac{\pi(2a \sin \theta)(\cos \theta)}{\frac{4a^2 \sin^2 \theta}{a}} = \frac{\pi}{2} \cot \theta = \delta, \text{ and,}$$

$$d\delta = -\frac{\pi}{2} \operatorname{cosec}^2 \theta \, d\theta = -\frac{\pi}{2} \frac{d\theta}{\sin^2 \theta} \tag{4}$$

Furthermore, $\sin \gamma = \frac{z-a}{a} = \frac{z}{a} - 1 = \frac{r^2}{2a^2} - 1 = \frac{4a^2 \sin^2 \theta}{2a^2} - 1 = 2\sin^2 \theta - 1$

$$= \sin^2 \theta + (\sin^2 \theta - 1) = \sin^2 \theta - \cos^2 \theta = -\cos 2\theta$$

$$\text{so, } \gamma = 2\theta + \frac{3\pi}{2}, \text{ and } d\gamma = 2\, d\theta. \tag{5}$$

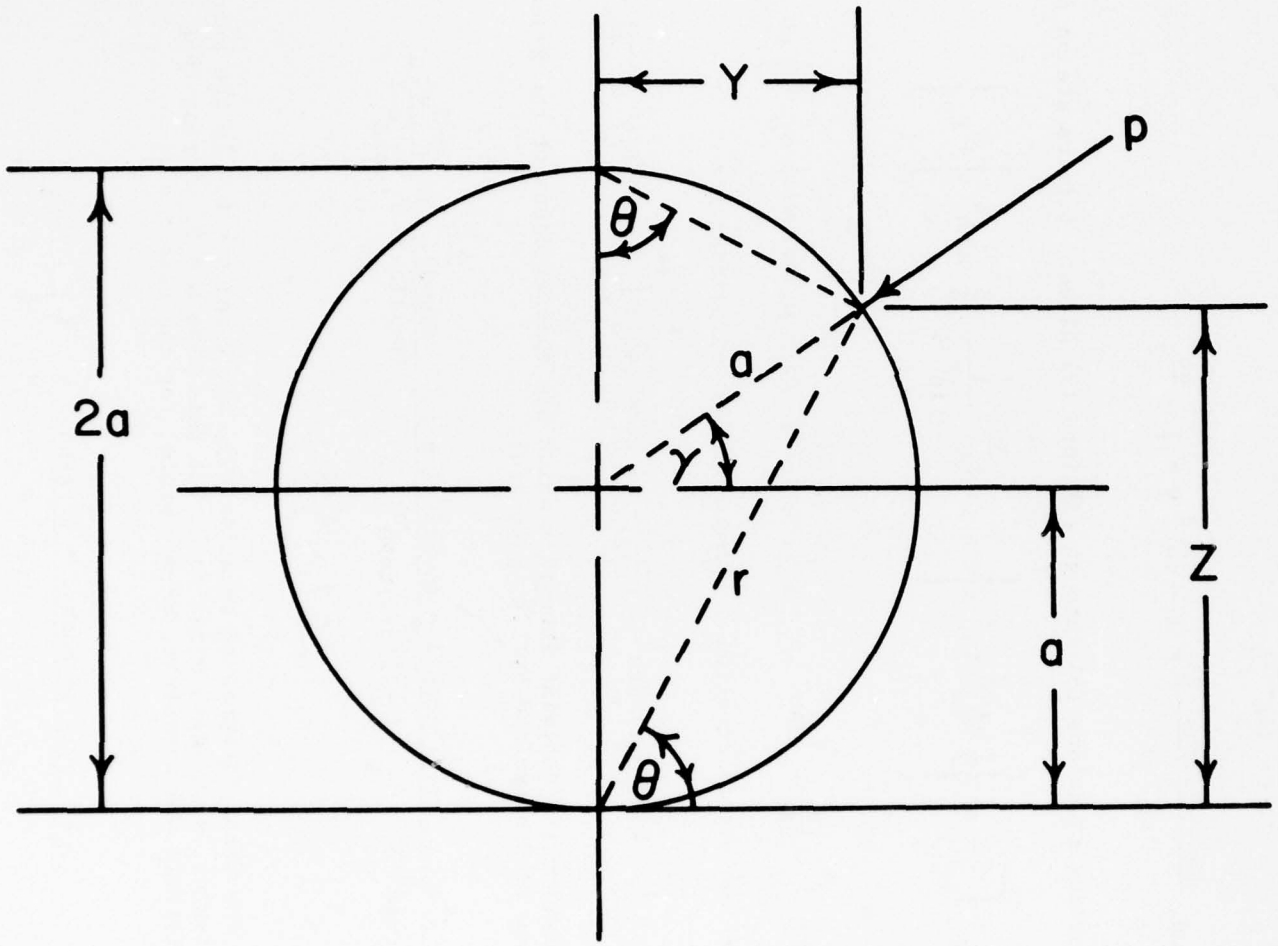

Figure 3. Coordinate system defining geometric parameters of interest.

Finally, $\dfrac{a^2\pi^4}{4z^2} = \dfrac{a^2\pi^4}{\frac{4r^4}{4a^2}} = \dfrac{a^4\pi^4}{16a^4\sin^4\theta} = \dfrac{\pi^4}{16\sin^2\theta\sin^2\theta} = -\dfrac{\pi^3}{8}\dfrac{1}{\sin^2\theta}\dfrac{d\delta}{d\theta}$ (6)

And, $\dfrac{\sin^2\theta - \cos^2\theta}{\sin^2\theta} = 1 - \cot^2\theta = 1 - \dfrac{4\delta^2}{\pi^2}$ (7)

Putting equations (3) through (7) into (2) gives: (Limits are on δ)

$$f_z = \int_{+\infty}^{-\infty} -(a)\left\{\frac{1}{2}\rho U_o^2 \sin^2\alpha\left[1 - (-\frac{\pi^3}{8})\frac{1}{\sin^2\theta}\frac{d\delta}{d\theta}\operatorname{sech}^4\delta\right] + p_o\right\}$$

$$[-\cos 2\theta]2\, d\theta \qquad (8)$$

Now, $\int_{-\pi}^{o} -[\frac{a}{2}\rho U_o^2\sin^2\alpha + p_o][-\cos 2\theta]2\, d\theta = 0$, so, with $q_o = \frac{1}{2}\rho U_o^2\sin^2\alpha$ and the use of equation (7), equation (8) simplifies to:

$$f_z = \int_{+\infty}^{-\infty} 2(aq_o\frac{\pi^3}{8})\operatorname{sech}^4\delta\,[\frac{4\delta^2}{\pi^2} - 1]\, d\delta = -aq_o\pi\int_{-\infty}^{+\infty}\operatorname{sech}^4\delta[\delta^2 - \frac{\pi^2}{4}]\, d\delta \qquad (9)$$

Equation (9) contains integrals which are special cases of the general form (see Gradshteyn and Ryzhik, page 124):

$$\int\frac{\delta^m d\delta}{\cosh^n\delta} = \frac{m\delta^{m-1}\cosh\delta + (n-2)\delta^m\sinh\delta}{(n-1)(n-2)\cosh^{n-1}\delta} - \frac{m(m-1)}{(n-1)(n-2)}\int\frac{\delta^{m-2}d\delta}{\cosh^{n-2}\delta} + \frac{n-2}{n-1}\int\frac{\delta^m d\delta}{\cosh^{n-2}\delta} \qquad (10)$$

In the first integral of equation (9), $m = 2$ and $n = 4$. In the second integral, n is again equal to 4, but this time $m = 0$. Noting that the integrals are symmetric, we may write, for the case $m = 2$:

$$\int_o^\infty \delta^2\operatorname{sech}^4\delta\, d\delta = [\frac{\delta\cosh\delta + \delta^2\sinh\delta}{3\cosh^3\delta}]_o^\infty - \frac{1}{3}\int_o^\infty\frac{d\delta}{\cosh^2\delta} + \frac{2}{3}\int_o^\infty\frac{\delta^2 d\delta}{\cosh^2\delta} \qquad (11)$$

The first term on the right hand side of equation (11) evaluates to zero by application of L'Hospital's rule. The second integrates to $\tan \delta \Big|_o^\infty = 1$ (see Gradshteyn and Ryzhik, page 99) and the third integral is of the form (Gradshteyn and Ryzhik, page 353): $\int_o^\infty \frac{\delta^{2k} d\delta}{\cosh^2 b\delta}$

$= \frac{(2^{2k} - 2)\pi^{2k}}{b(2b)^{2k}} |B_{2k}|$, which, for k=1=b evaluates to $\frac{\pi^2}{12}$ with the Bernoulli number $|B_2| = \frac{1}{6}$. Putting all of this together, the first integral of equation (9) may be evaluated in closed form to yield $(\pi^2 - 6)/9$. Now, for the case m = 0, equation (10) becomes:

$$\int_o^\infty \operatorname{sech}^4 \delta \, d\delta = \left[\frac{\sinh\delta}{3\cosh^3 \delta}\right]_o^\infty + \frac{2}{3} \int_o^\infty \frac{d\delta}{\cosh^2 \delta} \qquad (12)$$

As before, the first term on the right hand side of equation (12) evaluates to zero, and the second term integrates to unity. Thus, the second integral of equation (9) may be evaluated in closed form to yield $(4/3)(-\pi^2/4)$. We may then write:

$$f_z = -aq_o\pi\left[\frac{\pi^2-6}{9} - \frac{4\pi^2}{12}\right] = \frac{-aq_o\pi}{9}\left[-2\pi^2 - 6\right] = 9aq_o \qquad (13)$$

Note the positive resultant sign of equation (13), indicating that the net force per unit length of limb is in the positive z-direction, or tending to cause dislodgement of the limb from a restraining surface (which could also be another limb).

In order to evaluate equation (13) further, we need to say something about q_o and a. As a reasonable approximation, we may begin by assuming that the radius of the human forearm is on the order of 1.5 inches (average) and that the length of this portion of the arm is about one foot. Thus, the <u>total</u> force acting on the forearm can be approximated by the relation $f_t = \frac{9}{8} q_o$. Now, consider an ejection taking place at an altitude of 10,000 feet. At this height, the density of air relative to a known standard is given by (Shames, page 540) $\frac{\rho}{\rho_o} = 0.7385$, where $\rho_o = 0.002378$ slug/ft^3, and the speed of sound, c = 1,078 feet per second. Thus, $q_o = \frac{1}{2}\frac{\rho}{\rho_o}\rho_o[U_o^2/c^2]c^2\sin^2\alpha = 1020M^2\sin^2\alpha$, where M corresponds to the Mach Number of the flow. Substituting this result into the equation for f_t gives the total limb-dislodging force as a function of Mach Number

and Angle of Attack at the specified altitude of 10,000 feet. The final equation is:

$$f_t = 1148\ M^2 \sin^2\alpha \qquad (14)$$

Figure 4 shows equation (14) plotted as limb dislodging force vs. Mach Number with the angle of attack appearing as a parameter. Although the figure illustrates force behavior in the supersonic range as well as the subsonic, it is recognized that the results past M = 1 are not realistic, since the analysis has thus far neglected the presence of any shock waves in the flow. In any case, the subsonic values for f_t are, in themselves, very revealing. For example, at the higher angles of attack one observes a rapidly increasing limb-dislodging force. The significance of these large forces may be appreciated by examining them in relation to the super-imposed ordinate axis which is a measure of several published probability results. That is, in a study conducted by Horner and Hawker (1973) it was found that a pilot's average grip retention is such that the probability of his letting go is 100% if the dislodging force exceeds some 600 pounds. From Figure 4, we see that f_t = 600 pounds when M = .72 for $\alpha = 90°$ and when M = .83 for $\alpha = 60°$. Thus, at these higher angles of attack a pilot's musculo-skeletal system is not likely to withstand the tendency for dislodgement from a restraining surface if he is ejecting at Mach Numbers in excess of around 0.7. Similarly, in a study conducted by Payne (1975) it was found that the probability of major flail injury is around 100% if the ejection Mach Number exceeds 1.25. This would appear to be self-consistent with the predicted limb dislodging forces as interpreted above together with the results of Horner and Hawker. To this level of approximation, therefore, one would have to conclude that the generation of stagnation points in the flow produces forces that can cause limb-dislodgement (with subsequent flail and possible serious injury). Moreover, these forces are sensitive to the angle at which the limb intercepts the flow, such that the higher the angle, the greater the tendency for dislodgement. And finally, the forces increase rapidly with speed of ejection, which correlates well with the finding that windblast injuries increase dramatically as a function of airspeed (Glaister, 1975). Figure 5, taken from Payne, Hawker and Euler (1975) is a photograph of an ejection seat occupant sitting in the ACES-II Seat at -15° Yaw and -15° Pitch, during a wind-tunnel simulation of an ejection from the F-105. The arrows point out several critical regions of the pilot-ejection-seat configuration where flow stagnation, with its consequent limb-dislodging force distribution, is likely to occur. Observe, in particular, those regions where the pilot is gripping the seat, where his upper arms are in contact with his torso, where the lower legs are in contact with the seat pan and where his head is in contact with the back of the seat. All of these represent sites of potentially serious windblast and flail injury. Based on these results, one is therefore encouraged to pursue the mathematical analysis with a certain degree of assurance that the approach is faithfully describing events as they have been experimentally observed to take place. With this in mind, we now proceed to modify the theory to include flow separation effects.

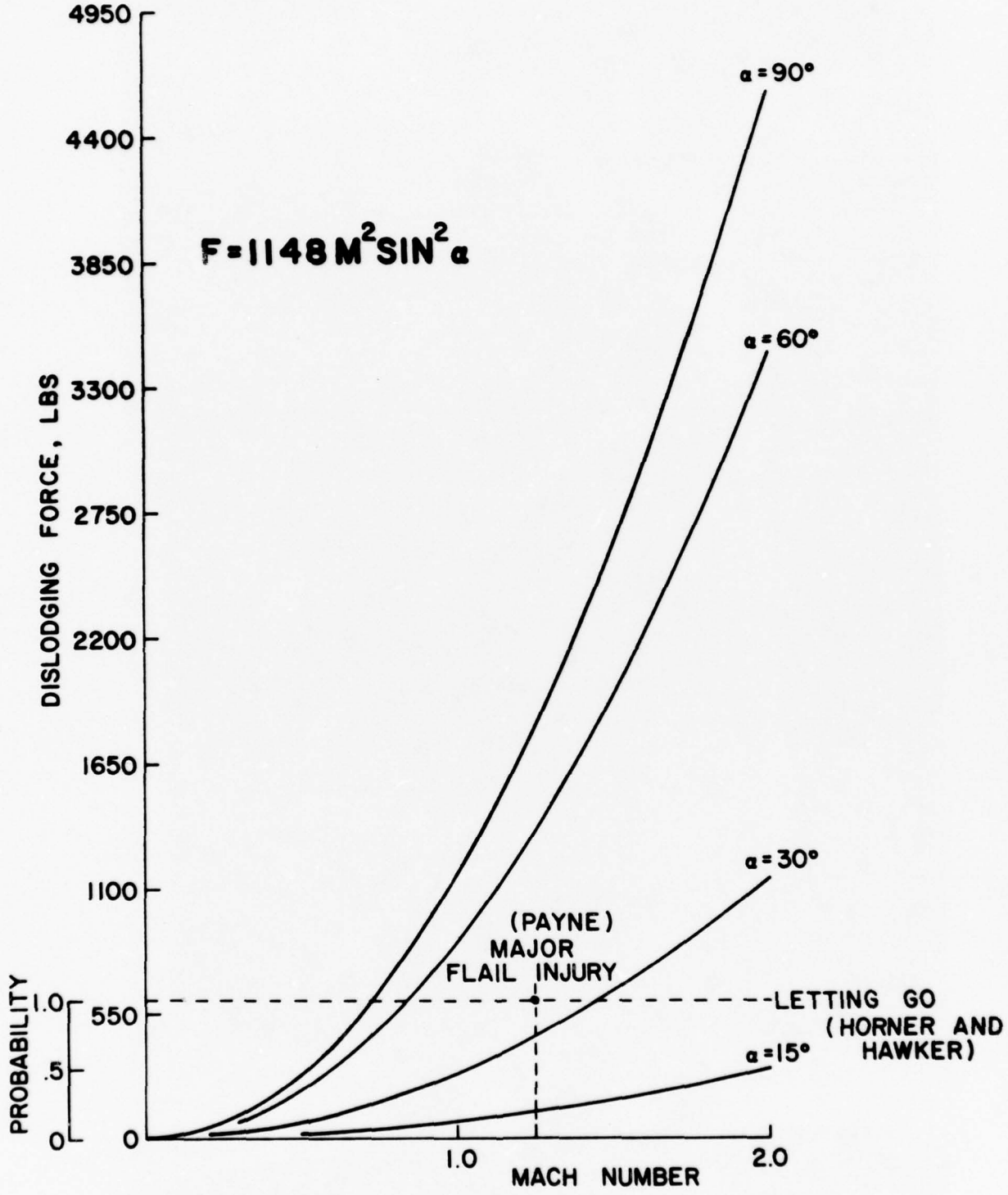

Figure 4. Limb Dislodging Force vs. Mach Number of Ejection

Figure 5. Some sites of flow stagnation for an ejection seat occupant sitting in the ACES-II Seat (See arrows).

SECTION III

VORTEX MOTION IN A REGION OF SEPARATION

In aerodynamic flow theory, two simplifications have been conveniently and commonly employed to investigate separated flows over arbitrary three dimensional bodies of revolution (Marshall and Deffenbaugh, 1975). The first asserts that there is a direct analogy between three-dimensional steady flow and two-dimensional unsteady flow (Allen and Perkins, 1951) -- such that a three-dimensional steady separated flow problem can be analyzed as a two-dimensional unsteady separated flow problem. The second is based upon the observation (verified experimentally) that a two dimensional unsteady wake can be described by a distribution of inviscid vortices, originating from the separation of shear layers and superimposed on the unseparated potential flow solution (Mello, 1959, Sarpkaya, 1968 and Marshall and Deffenbaugh, 1975). These vortices are modified by diffusion. It is the second of these two assumptions that we shall exploit here, since arguments have already been presented for considering flow over the forearm in contact with a restraining surface to be two-dimensional (Schneck, 1976).

Thus, to examine the separated flow patterns around the geometric configuration illustrated in Figure 2, consider the situation depicted in Figure 6. A Vortex pair has been placed on the lee or downstream side of the two cylinders as shown. Neither the location, $y_o \pm iz_o$, nor the strength, κ, of these two vortices can be specified at this time. In fact, the location of the vortex pair can <u>not</u> be determined uniquely from potential flow theory alone (see later discussion). However, the vortex strength <u>can</u> be computed if we say something about how these vortices move relative to the cylinders. In this respect, reasoning developed in the earlier report (Schneck, 1976) has suggested that, during the first few milliseconds of high-speed flow development around a blunt body of revolution, the separated wake stays confined to the immediate region of the body, and consists essentially of two thin vortex-layers, symmetrically situated. One may thus model this separated flow analytically by super-imposing stationary vortex filaments upon the linear inviscid flow solutions obtained earlier. The condition of stationarity then allows the vortex strength to be determined as described later in this report.

Derivation of Complex Velocity Potential for a Vortex Pair Downstream of Two Tangent Cylinders with Parallel Axes

In order to super-impose the vortex layers on the earlier solutions, as described above, we must first develop a complex velocity potential to describe the vortex pair illustrated in Figure 6. The analytic form for this potential can be deduced in part by examining the transformation that maps the double cylinder configuration of Figure 6 into a single unit circle centered at the origin of the transformed plane (see Carrier, Krook and Pearson, 1966, pgs. 132-134). Consider the bilinear trans-

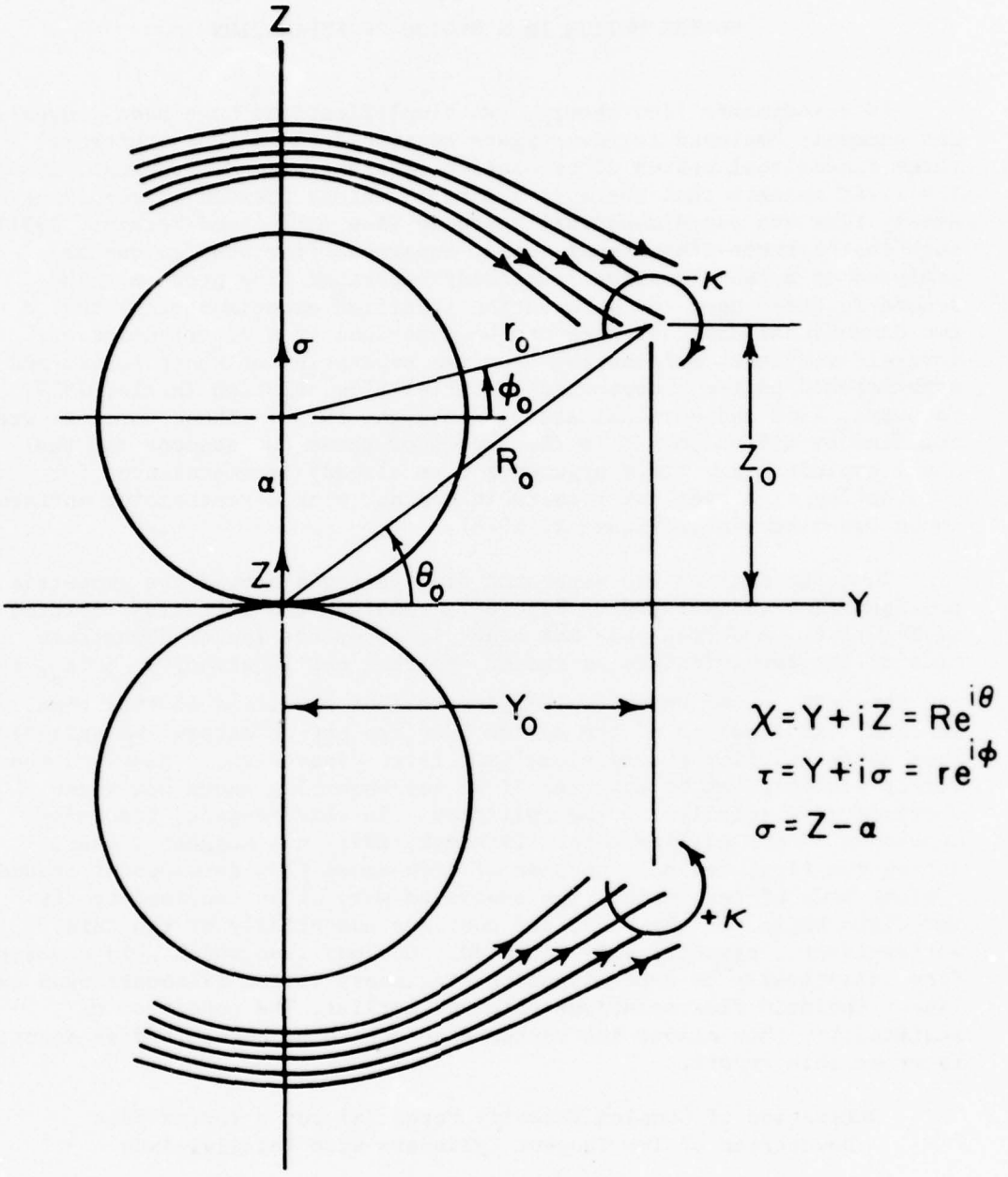

Figure 6. Schematic Representation of Vortex Pair Downstream of Two Tangent Circular Cylinders.

formation:

$$u + iv = \frac{i\chi - 2}{\chi} = \frac{i\chi\bar{\chi} - 2\bar{\chi}}{\chi\bar{\chi}} = \frac{i(y^2 + z^2) - 2(y - iz)}{y^2 + z^2}. \qquad (15)$$

On the upper cylinder of Figure 6, with a = 1, the equation of the circle is $y^2 + z^2 = 2z$. Substituting this into equation (15), we find that v = 2 = constant for any value of u. Similarly, on the lower cylinder, $y^2 + z^2 = -2z$, yielding v = 0 for any value of u. The bilinear transformation (15) thus maps the two tangent circles, S_1 and S_2 of Figure 6 into the parallel lines v = 2 and v = 0, respectively, in the u, v plane. This is illustrated in Figure 7A.

Next, consider the exponential transformation:

$$x + is = e^{\frac{\pi}{2}(u + iv)} = e^{\frac{\pi}{2}u}\, e^{\frac{\pi}{2}iv} = e^{\frac{\pi}{2}u}\,(\cos\tfrac{\pi}{2}v + i\sin\tfrac{\pi}{2}v). \qquad (16)$$

For v = 2, s = 0 and $x = -e^{(\pi/2)u}$ which maps S_1 onto the negative real axis of the x,s plane. Likewise, for v = 0, s = 0 and $x = +e^{(\pi/2)u}$ which maps S_2 onto the positive real axis of the x,s plane. The exponential transformation (16) thus maps the two parallel lines of Figure 7A onto the real axis of the x,s plane, as illustrated in Figure 7B.

Finally, consider the inverse bilinear transformation:

$$\xi + i\eta = \frac{x + is + i}{x + is - i} = \frac{x + i}{x - i} = \frac{(x + i)(x + i)}{(x - i)(x + i)} = \frac{x^2 + 2ix - 1}{x^2 + 1}, \qquad (17)$$

where s has been set equal to zero in accordance with the discussion of equation (16). From equation (17) we get $\xi = (x^2 - 1)/(x^2 + 1)$ and

$\eta = 2x/(x^2 + 1)$. Thus, $\xi^2 + \eta^2 = \dfrac{x^4 - 2x^2 + 1 + 4x^2}{(x^2 + 1)^2} = \dfrac{x^4 + 2x^2 + 1}{x^4 + 2x^2 + 1} = 1,$

so that, for s = 0 equation (17) defines the equation of a circle of radius 1 in the ξ,η plane. The inverse transformation (17) thus maps the real axis of the x,s plane into a unit circle centered at the origin in the ξ,η plane, as illustrated in Figure 7C.

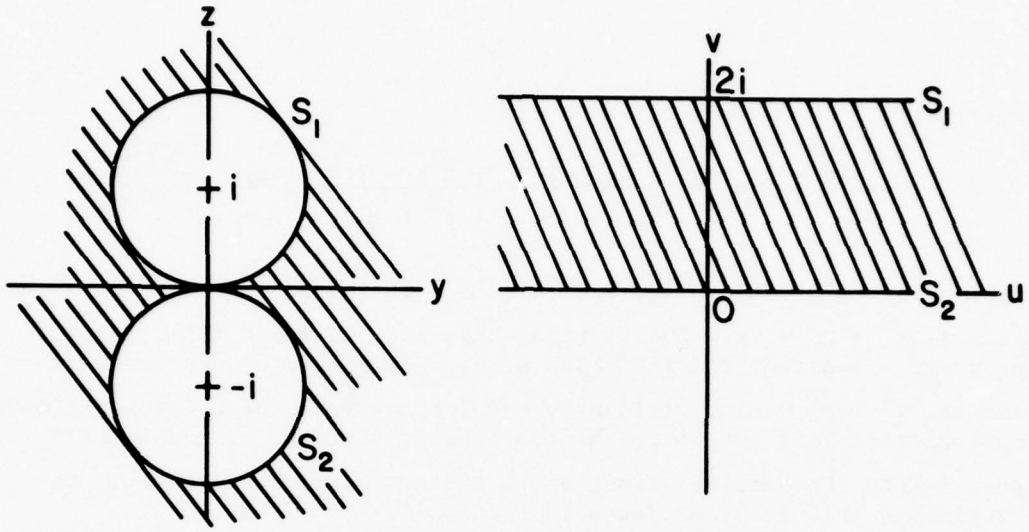

Figure 7A: Bilinear Transformation $u + iv = \frac{i(y^2 + z^2) - 2(y - iz)}{y^2 + z^2}$

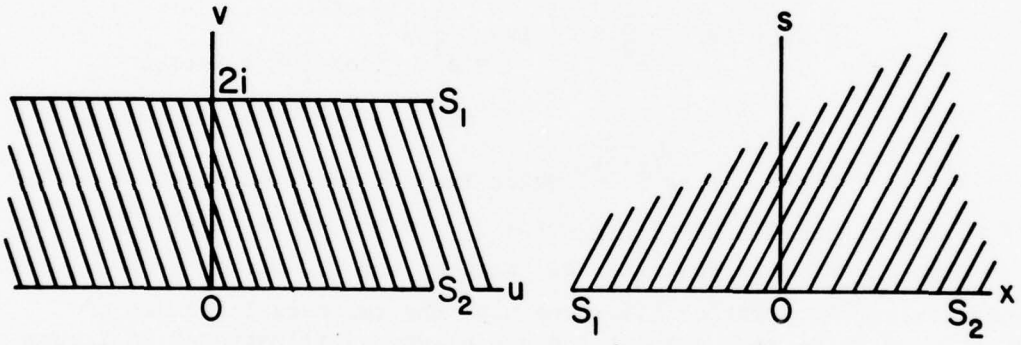

Figure 7B: Exponential Transformation $x + is = e^{\frac{\pi}{2}u} (\cos \frac{\pi}{2}v + i \sin \frac{\pi}{2}v)$

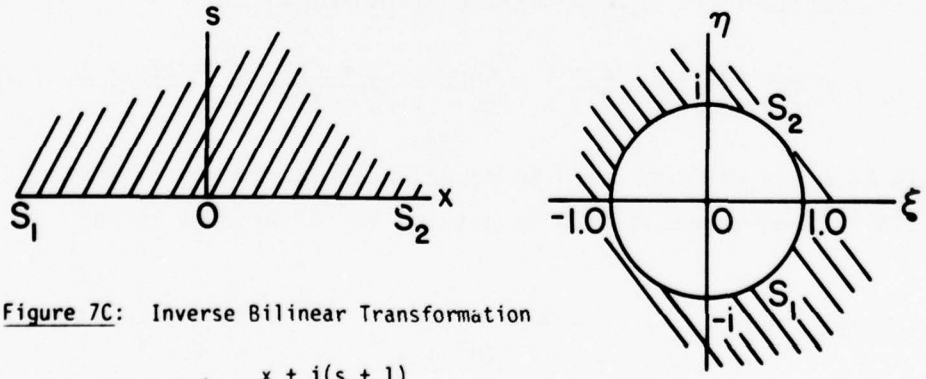

Figure 7C: Inverse Bilinear Transformation

$$\xi + i\eta = \frac{x + i(s + 1)}{x + i(s - 1)}$$

Figure 7. Transformation of Two Unit Cylinders tangent on the real axis to a Single Unit Cylinder centered at the Origin.

Now, putting together the transformations (15), (16) and (17), one obtains the single function that maps the two unit cylinders of Figure 7A into the single unit circle of Figure 7C. Thus,

$$W = \xi + i\eta = \frac{x + is + i}{x + is - i} = \frac{e^{\frac{\pi}{2}(u + iv)} + i}{e^{\frac{\pi}{2}(u + iv)} - i} = \frac{e^{\frac{\pi}{2}\frac{(i\chi - 2)}{\chi}} + e^{\frac{\pi}{2}i}}{e^{\frac{\pi}{2}(\frac{i\chi - 2}{\chi})} - e^{\frac{\pi}{2}i}}$$

$$= \frac{e^{-\frac{\pi}{\chi}} + 1}{e^{-\frac{\pi}{\chi}} - 1}. \tag{18}$$

By multiplying the top and bottom of the quotient in equation (18) by the quantity $e^{+(\pi/2\chi)}$, the mapping function may be put into the form:

$$W = -\frac{e^{-\frac{\pi}{2\chi}} + e^{+\frac{\pi}{2\chi}}}{e^{+\frac{\pi}{2\chi}} - e^{-\frac{\pi}{2\chi}}} = -\coth\left(\frac{\pi}{2\chi}\right). \tag{19}$$

Figure 8 illustrates the net transformation represented by equation (19). The significance of this transformation is that it suggests an analytic form for the complex potential when inviscid flows encounter boundaries such as those depicted in Figures 2, 6 or 8. For example, let us expand equation (19) into its real and imaginary parts and see what information can be gained from the results obtained. Expansion of the hyperbolic cotangent of complex argument yields the following:

$$\coth\left(\frac{\pi}{2\chi}\right) = \coth\left(\frac{\pi\bar{\chi}}{2\chi\bar{\chi}}\right) = \coth\frac{\pi(y - iz)}{2(y^2 + z^2)} = \frac{\sinh\frac{\pi y}{r^2} - i\sin\frac{\pi z}{r^2}}{\cosh\frac{\pi y}{r^2} - \cos\frac{\pi z}{r^2}}$$

$$= A_1(y,z) + iA_2(y,z) = A_3(y,z)e^{i\beta(y,z)} \tag{20}$$

where: $A_1(y,z) = \dfrac{\sinh\frac{\pi y}{r^2}}{\cosh\frac{\pi y}{r^2} - \cos\frac{\pi z}{r^2}}$; $A_2(y,z) = \dfrac{-\sin\frac{\pi z}{r^2}}{\cosh\frac{\pi y}{r^2} - \cos\frac{\pi z}{r^2}}$;

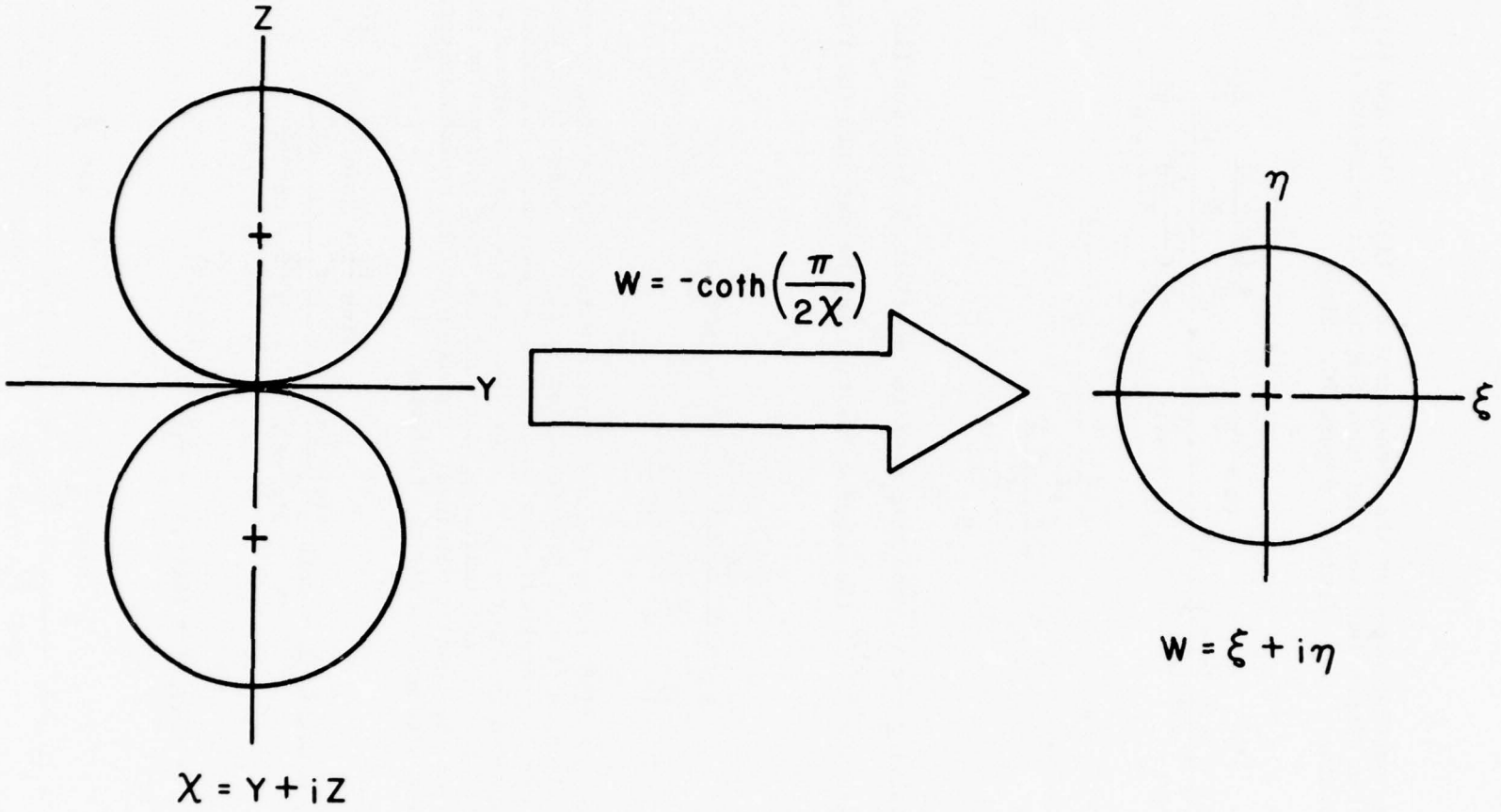

Figure 8. Mapping Function to Transform a Double-Cylinder Configuration into a Corresponding Single Cylinder Centered at the Origin.

$$A_3(y,z) = \sqrt{A_1^2(y,z) + A_2^2(y,z)}; \text{ and, } \beta(y,z) = \text{Arc Tan } \frac{A_2(y,z)}{A_1(y,z)}$$

Now observe that if $r^2 = 2z$ (the equation of the upper cylinder in Figures 2 or 8) then $A_1(y,z) = (\sinh \frac{\pi y}{2z})/(\cosh \frac{\pi y}{2z})$ and $A_2(y,z) = (-1)/(\cosh \frac{\pi y}{2z})$, so

$$\text{that: } A_3^2(y,z) = A_1^2(y,z) + A_2^2(y,z) = \frac{(\sinh \frac{\pi y}{2z})^2 + 1}{(\cosh \frac{\pi y}{2z})^2} = \frac{\cosh^2 \frac{\pi y}{2z}}{\cosh^2 \frac{\pi y}{2z}} = 1.$$

The exact same statement can be made for the lower cylinder which is defined by the equation $r^2 = -2z$ because the negative sign disappears when $A_1(y,z)$ and $A_2(y,z)$ are squared in the calculation of $A_3(y,z)$. The modulus of equation (20) is thus equal to 1 on the boundary defined by figures 2 or 8. Moreover, the logarithm of this modulus is therefore equal to zero on this particular boundary. Consequently, we conclude that the quantity represented by the logarithm of the modulus of equation (20) could represent the stream function for flow around a double-cylinder geometric configuration such as that being considered here. In fact, upon plotting this logarithm, we find that it corresponds to a circulation pattern around just such a double cylinder configuration. This is illustrated in Figure 9.

To summarize, up to this point it has been shown that if we take the log of both sides of equation (20), the real part of the right hand side, i.e., $\log A_3(y,z)$ represents the streamline pattern for fluid circulation around a boundary consisting of two unit cylinders tangent to one another as shown in Figures 2, 8 and 9. This log function should therefore correspond to the stream function, Ψ, of the complex velocity potential suggested by equations (19) and (20). In order to affect this correspondence we must multiply the log of equation (20) by the quantity i, so that $\log A_3(y,z)$ will now become the imaginary part of the complex potential $w = \Phi + i\Psi$, and thus correctly represent a stream function. Finally, to designate some strength to the circulation pattern, we assign some arbitrary parameter K to the complex velocity potential giving the result:

$$w = iK \log [\coth (\frac{\pi}{2\chi})] \qquad (21)$$

The imaginary part of equation (21) now yields a circulation streamline pattern (Figure 9) around the boundaries defined by the equation $r^2 = \pm 2z$. This circulation pattern is a measure of the strength of vortices which are downstream of the boundaries, and, in fact, is directly proportional by a factor of 2π to the magnitude, κ, or vortex strength of the

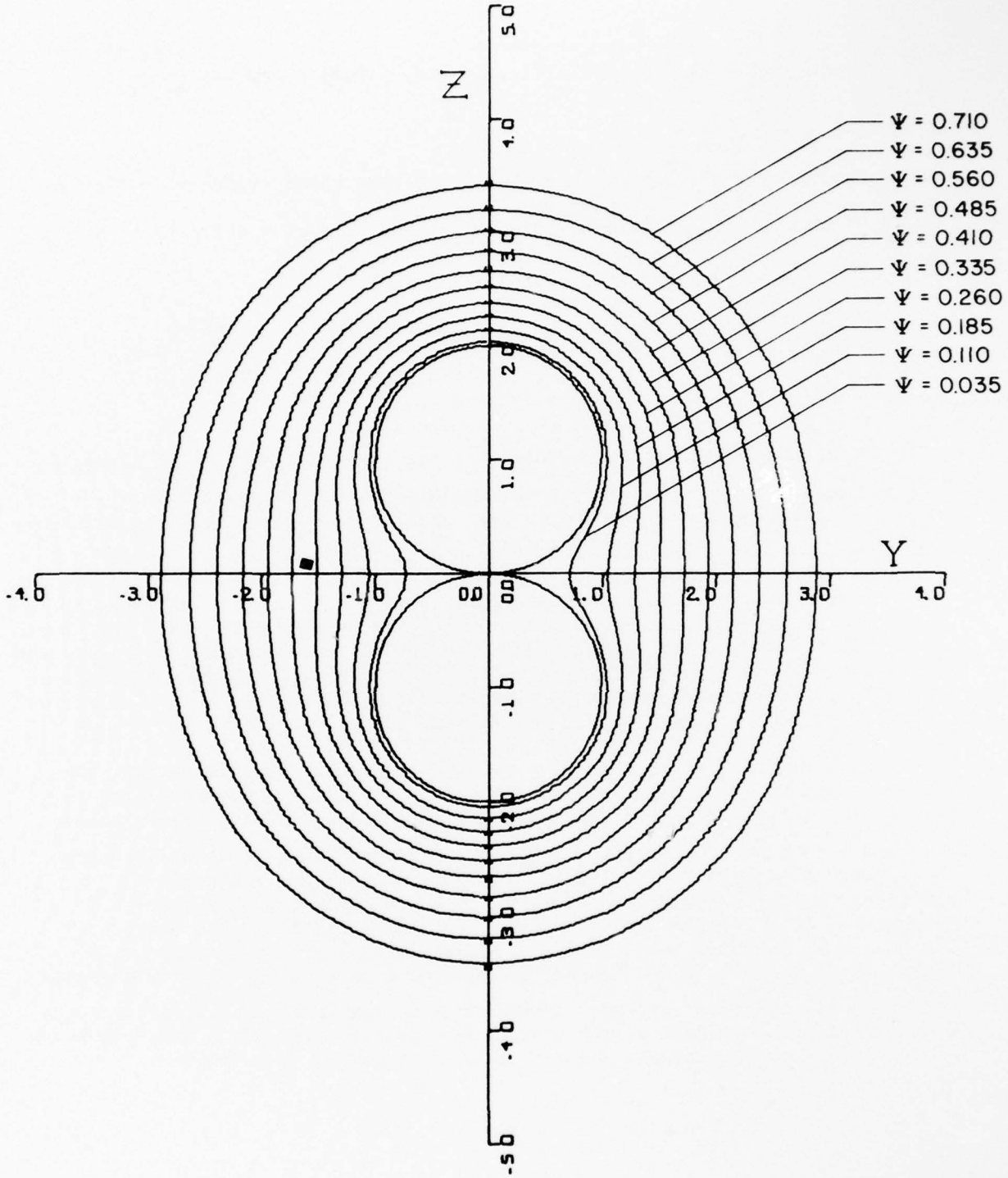

Figure 9. Circulation Pattern around a Double-Cylinder Configuration. The Non-dimensionalized Stream Functions for this Circulation Pattern are given by the logarithm of Equation (20) defined in the text.

vortex pair defined by the complex velocity potential:

$$w = i\kappa \log \frac{\chi - \bar{\chi}_o}{\chi - \chi_o} \tag{22}$$

Thus, we conclude that the vortex pair on the downstream side of the cylinders illustrated in Figure 6 may be defined by the stream function:

$$\Psi = \frac{1}{2\pi} \text{Im} \{iK \log [\coth (\frac{\pi}{2\chi})]\} \text{Im} [i \log \frac{\chi - \bar{\chi}_o}{\chi - \chi_o}] \tag{23}$$

Note, in equation (23), that K (a real constant) and the location, $y_o \pm iz_o$ are still undefined. In any event, we may plot $(2\pi\Psi/K)$ for arbitrary y_o and z_o just to get an idea of what the streamline patterns look like. This is done in Figure 10 for a vortex pair placed at $y_o = 1.6$ and $z_o = \pm 1.6$.

Determination of Circulation Strength

It was mentioned earlier that the strength, K, of the circulation pattern could be computed if we say something about how the vortex pair moves relative to the cylinders. More specifically, reasoning has been presented for assuming that early in the flow-development process the separated wake stays confined to the immediate region of the cylinders, and that the vortex layers therefore remain stationary with respect to these cylinderical bodies. Stating this fact mathematically allows K to be determined as follows: suppose the flow we are examining consists of a cross-flow pattern having streamlines defined by the imaginary part of equation (1), and vortices defined by the stream functions of equation (23). Then, the cross-flow would, for K arbitrary, have a tendency to carry the vortex pair along with it, so that these would be shed <u>downstream</u> as a function of time. Moreover, each vortex would, itself, have a tendency to induce a translational velocity at the center of its corresponding partner. In fact, for the situation shown in Figure 6, note that the velocity field induced by each vortex on the other has a tendency to cause the vortex pair to drift <u>upstream</u>. Now, if we impose the stationarity condition as described earlier, then, by requiring the <u>downstream</u> velocity of the vortex pair to exactly balance the <u>upstream</u> velocity, we find that K no longer becomes arbitrary but takes on a value determined uniquely by the condition of stationarity. The velocity induced at $y_o + iz_o$ by the complex velocity potential given in equation (1) is $(dw/d\chi)$ evaluated at y_o, z_o. Similarly, the velocity induced at $y_o + iz_o$ by the stream function given in equation (23) is

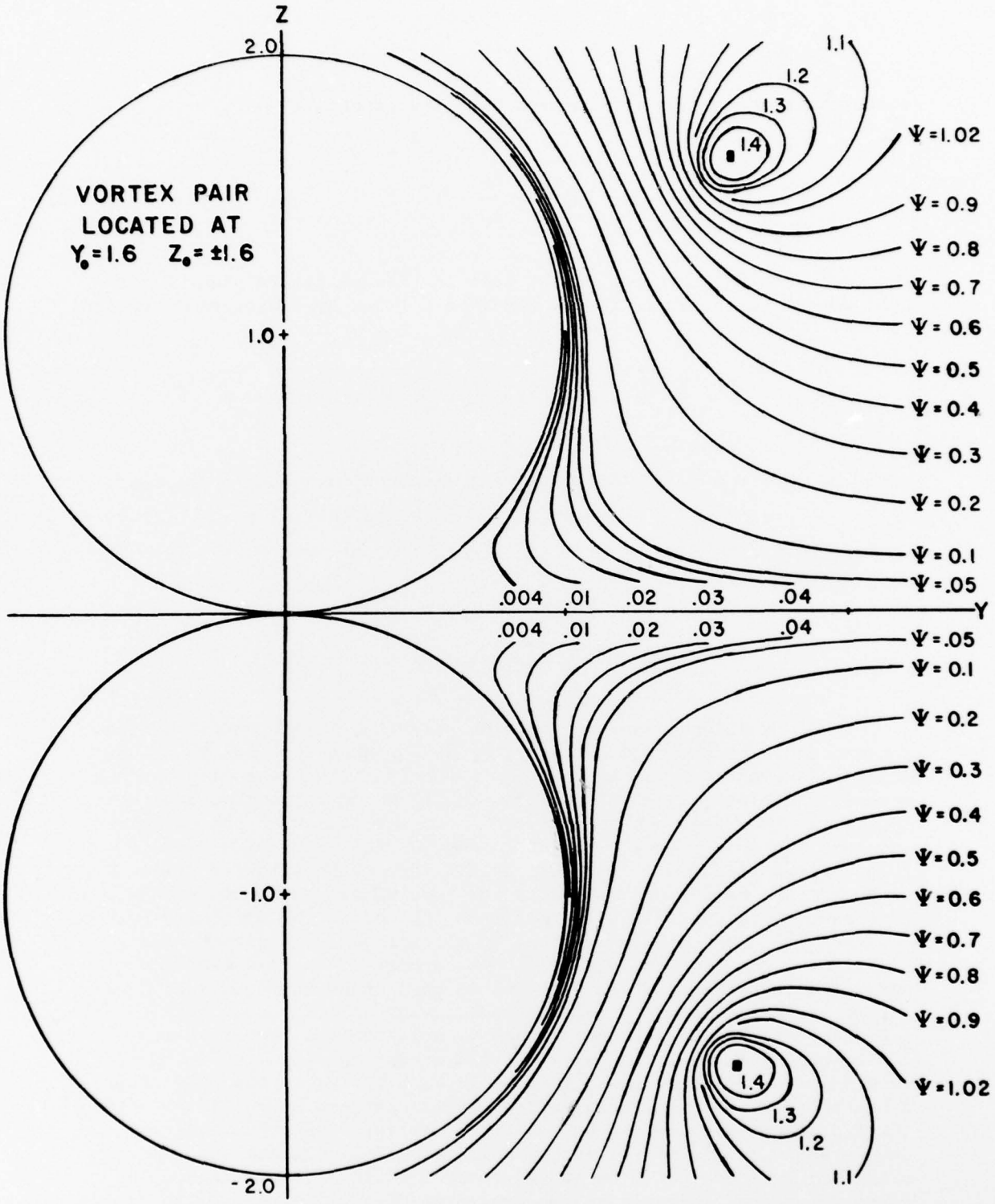

Figure 10. Non-dimensional Streamline Patterns for Vortex Pair in The Vicinity of Two Tangent Cylinders. Note: All Stream Functions Below the Axis z = 0 are Negative

$(-\partial\Psi/\partial z) + i(\partial\Psi/\partial y)$ also evaluated at y_o, z_o. Adding these two velocities together and setting their sum equal to zero thus insures stationarity of the vortex pair and gives a relationship between the circulation strength, K, the cross-flow velocity, V, and the vortex locations $y_o \pm iz_o$. At this point, however, we cannot pursue the analysis any further until y_o and z_o are somehow quantitatively defined.

Potential flow theory alone can provide no information concerning the location of vortices in a separated wake. Such information must be determined either by considering the variation of pressure across the boundary layer, as described by Sarpkaya (1968) and Bar-Lev and Yang (1975), or by performing a series of carefully designed experiments. It is our intent to exploit both of these techniques in future studies.

SECTION IV

CONCLUDING REMARKS

In this report, the mathematical model developed in an earlier work (Schneck, 1976) has been expanded upon in two ways. First, actual forces which tend to dislodge two limbs from one another, or from a restraining surface, have been calculated in the absence of flow separation. Second, the theory has been modified to allow for the inclusion of some physical effects attributable to separation of flow around the blunt body segments. It is clear from the results obtained thus far, that aircraft ejections taking place above Mach 0.8 have associated with them a very high probability of limb-flail injury. This would appear to be due to the forces generated as a consequence of the manner in which the ejection seat occupant intercepts the air stream. The generation of stagnation points in the flow leads to limb-dislodging forces which, beyond Mach 0.7, exceed the musculo-skeletal ability of the pilot to "hold on". This, then, becomes an important design criterion for ejection systems, i.e., to minimize stagnation of the flow as the pilot intercepts the air stream.

It is likely that flow separation also plays an important role in the generation of limb dislodging forces because this phenomenon is responsible for the major component of drag when a blunt body is placed in a high-speed fluid flow. It is thus important to quantify the effects of flow separation and it is anticipated that this will be done in future investigations -- both analytically and experimentally. Also to be examined in future studies is the time-course of limb dislodging forces. That is, the force distribution shown in Figure 4 exists at the onset of ejection and these are peak forces that prevail so long as the limb is in contact with a restraining surface. Once contact with the surface is broken, there follows a redistribution of forces, and this information is desirable input to the ATB simulation which provides kinematic data. All of this work is being carried out in an effort to define specific design criteria for safer ejections.

LIST OF SYMBOLS

$A_1(y,z)$ $\quad \dfrac{\sinh \frac{\pi y}{r^2}}{\cosh \frac{\pi y}{r^2} - \cos \frac{\pi z}{r^2}}$

$A_2(y,z)$ $\quad \dfrac{-\sin \frac{\pi z}{r^2}}{\cosh \frac{\pi y}{r^2} - \cos \frac{\pi z}{r^2}}$

$A_3(y,z)$ $\quad \sqrt{A_1^{\,2}(y,z) + A_2^{\,2}(y,z)}$

$|B_{2k}|$ Bernoulli Number of order 2k

C_p Surface Pressure Coefficient = $\dfrac{p - p_o}{\frac{1}{2}\rho U_o^{\,2}}$

F The same as f_t

K Circulation Strength around double-circular-cylinder configuration

M Mach Number = $\dfrac{U_o}{c}$

R_o $\quad \sqrt{z_o^{\,2} + y_o^{\,2}}$

$S_{1,2}$ Designates curves in space

U_o Magnitude of Free-Stream Air Flow Velocity

V Magnitude of the Cross-Flow Velocity

W	Mapping Function
a	Radius of circles tangent to y-axis; Average human forearm radius
b	Arbitrary Coefficient
c	Speed of Sound
d	Ordinary Differential Operator
e	Base for Natural Logarithms = 2.718281828
f	Magnitude of the radial force generated by the fluid pressure, p
f_t	Total vertical force tending to dislodge the human forearm from a surface (or other limb) with which it is in contact.
f_z	The component of radial force in the z-direction, per unit length perpendicular to the y-z plane.
i	$\sqrt{-1}$
k	arbitrary integer exponent or subscript
m	arbitrary integer exponent or subscript, independent of k
n	arbitrary integer exponent or subscript, independent of k and m
o	used as a subscript to designate free-stream conditions, or to locate specific points in space, or to specify reference quantities.
p	Aerodynamic Pressure
p_o	Reference Pressure

q_o $\frac{1}{2} \rho U_o^2 \sin^2 \alpha$

r Radial coordinate, $r^2 = y^2 + \sigma^2$

r_o Radial location of the center of a vortex

s Exponential Transformation Coordinate (See x below)

t Time Coordinate

u Bilinear Transformation Coordinate (See v below)

v Bilinear Transformation Coordinate for the transformation u + iv

w Complex Velocity Potential, $w = \Phi + i\Psi$

x Exponential Transformation Coordinate for the transformation x + is

y Coordinate axis perpendicular to the line along which two limbs are in tangent contact, or the line along which one limb is in tangent contact with a restraining surface, and lying within the restraining surface.

y_o the y-coordinate locating the center of a vortex.

z Coordinate axis orthogonal to y and the restraining surface, i.e., normal to the arm rest.

z_o The z-coordinate locating the center of a vortex

α The angle of attack of the free stream relative to the center-line of the limb.

$\beta(y,z)$ Arc Tan $\frac{A_2(y,z)}{A_1(y,z)}$

ϕ_o Azimuthal Location of Vortex = Arc Tan $\frac{z_o - a}{y_o}$

η Transformation Coordinate (See ξ below)

κ Vortex Strength

ρ Fluid Mass Density

ρ_o Reference Density

γ Azimuthal Coordinate, Tan $\gamma = \frac{z - a}{y}$

θ Inscribed Angle

θ_o Vortex Location = Arc Tan $\frac{z_o}{y_o}$

σ $z - a$

τ $y + i\sigma = re^{i\phi}$

ξ Inverse Bilinear Transformation Coordinate for the transformation $\xi + i\eta$.

δ $\frac{\pi}{2} \cot \theta$

χ $y + iz = Re^{i\theta}$

$\overline{\chi}$ $y - iz$

π 3.141592654

∞ Designates Infinity

Ψ Stream Function of the Flow

Φ Velocity Potential of the Flow

∂ Designates Partial Differentiation

3

APPENDIX

COMPUTER PROGRAMS FOR CALCULATING AND PLOTTING STREAM FUNCTIONS

A. NON-DIMENSIONALIZED STREAMING FLOW PATTERN

```
      DIMENSION G(4200),H(4200),LABEL(10),LABLE(10),N2(400)
      DATA LABEL(1)/'                                    Y '/
      DATA LABLE(1)/'                          Z '/
      Y=.5
      X=5.
      CALL SAXIS(X,Y,LABLE,-4,7.0,90.,1.,1.,1.,1.)
      X=0.
      CALL SAXIS(X,Y,LABEL,-4,10.,0.,-5.,1.,1.,0.0)
      CALL CIRCLE(5.,1.5,1.)
      PI=355./113.
      DO 9 N=1,31,2
      PSIB=0.1*N
      PSIU=PSIB+.005
      PSIL=PSIB-.005
      N1=0
      DO 4 J=1,400
      Y=.025*(J-1)-5.0
      N2(J)=0
      I1=166
      IF(Y.GT.-2.0.AND.Y.LT.2.0)I1=500
      DO 5 I=1,I1
      IF(Y.GT.-2.0.AND.Y.LT.2.0)GO TO 7
      Z=.030*I
      GO TO 10
    7 Z=.010*I
   10 IF(((Z-1)*(Z-1)+Y*Y).LT.1)GO TO 5
      RSQ=Y*Y+Z*Z
      IF(RSQ.EQ.0.0)GO TO 5
      Q=RSQ-Z/2
      IF(Q.GT.-.01.AND.Q.LT..01)GO TO 5
      F1Y=PI*Y/RSQ
      F1Z=PI*Z/RSQ
      IF(ABS(F1Z-1.5708).LT.0.001)GO TO 5
      F2=TAN(F1Z)
      F3=COSH(F1Y)
      F4=TANH(F1Y)
      PSI=PI*F2/((F3*F3)*(F4*F4+F2*F2))
      IF(PSI.LE.0.)GO TO 5
      IF (PSI.LT.PSIL)GO TO 5
      IF (PSI.LT.PSIU.AND.PSI.GT.PSIL)GO TO 45
      GO TO 5
   45 N1=N1+1
      N2(J)=N2(J)+1
```

```
      IF(N2(J).GE.2) GO TO 92
      G(N1)=Y+5.
      H(N1)=Z+.5
      GO TO 5
   92 N1=N1-1
    5 CONTINUE
    4 CONTINUE
      CALL LINE(G,H,N1,+1)
    9 CONTINUE
      CALL PLOT(0.,0.,-4)
      STOP
      END
```

B. NON-DIMENSIONALIZED VORTEX PATTERN

```
      DIMENSION G(4200),H(4200),LABEL(10),LABLE(10),GG(3000),HH(3000)
     1,N2(400),Z1(600),W(402),Z2(1500)
      DATA LABEL(1)/'                                    Y '/
      DATA LABLE(1)/'                          Z '/
      DATA YO/1.6/,ZO/1.6/
      Y=.5
      X=5.
      CALL SAXIS(X,Y,LABLE,-.4,7.0,90.,1.,1.,1.,1.)
      X=0.
      CALL SAXIS(X,Y,LABEL,-4,10.,0.,-5.,1.,1.,0.0)
      CALL CIRCLE(5.,1.5,1.)
      PI=355./113.
      DO 9 N=1,31,2
      PSIB=0.1*N
      PSIU=PSIB+.005
      PSIL=PSIB-.005
      KK=1
      N1=0
      N3=0
      DO 4 J=1,400
      Y=.025*(J-1)-5.0
      N2(J)=0
      I1=166
      IF(Y.GT.0.00.AND.Y.LT.3.0)I1=500
      DO 5 I=1,I1
      IF(Y.GT.0.00.AND.Y.LT.3.0)GO TO 7
      Z=.030*I
      GO TO 10
    7 Z=.010*I
   10 W(J)=Z
      A4A=SQRT((Y-YO)**2+(Z-ZO)**2)
      B4=SQRT((Y-YO)**2+(Z+ZO)**2)
      IF(A4A.EQ.0.0)PSI=1000
      IF(A4A.EQ.0.0)GO TO 5
      E4=B4/A4A
      IF(E4.EQ.0.0)PSI=1000
      IF(E4.EQ.0.0)GO TO 5
      PSI=ALOG(E4)
      IF(PSI.LE.0.)GO TO 5
      IF (PSI.LT.PSIL)GO TO 5
      IF (PSI.LT.PSIU.AND.PSI.GT.PSIL)GO TO 45
      GO TO 5
   45 N1=N1+1
      Z1(1)=W(J)
      N2(J)=N2(J)+1
      IF(N2(J).GE.2)GO TO 92
      IF(N.EQ.1.AND.KK.EQ.2)GO TO 12
```

```
      IF(ABS(Z1(KK)-W(J)).GT.0.30)GO TO 92
   12 KK=KK+1                                                          2
      Z1(KK)=W(J)
      G(N1)=Y+5.
      H(N1)=Z+.5
      GO TO 5
   92 N1=N1-1
      IF(ABS(Z1(KK)-W(J)).LE.0.05)GO TO 5
      N3=N3+1
      Z2(1)=1000
      IF(ABS(Z2(N3)-W(J)).LE.0.05)GO TO 8
      Z2(N3)=W(J)
      GG(N3)=Y+5
      HH(N3)=Z+.5
      GO TO 5
    8 N3=N3-1
    5 CONTINUE
    4 CONTINUE
      CALL LINE(G,H,N1,+1)
      IF(N3.LE.2)GO TO 9
      CALL LINE(GG,HH,N3,+1)
      WRITE(6,50)N1,N3,PSIB
   50 FORMAT(6X,I4,2X,I4,2X,F10.3)
    9 CONTINUE
      CALL PLOT(0.,0.,-4)
      STOP
      END
```

C. NON-DIMENSIONALIZED CIRCULATION PATTERN

```
      DIMENSION G(4200),H(4200),LABEL(10),LABLE(10),N2(500)
      DATA LABLE(1)/'   '/
      DATA LABEL(1)/'   '/
      Y=0.5
      X=5.
      CALL SAXIS (X,Y,LABLE,-4,10.,90.,-5.,1.,1.,0.)
      X=1.0
      Y=5.5
      CALL SAXIS(X,Y,LABEL,-4,8.0,0.0,-4.,1.,1.,0.)
      CALL CIRCLE(5.,4.5,1.)
      CALL CIRCLE(5.,6.5,1.)
      PI=355./113.
      DO 15 L=1,2
      F=1.0
      IF(L.EQ.2)F=-1.0
      DO 9 N=7,152,15
      PSIB=N*.005
      PSIL=PSIB-.01
      PSIU=PSIB+.01
      N1=0
      DO 4 J=1,350
      Y=0.02*(J-1)-3.5
      N2(J)=0
      I1=120
      IF(Y.GT.-1.2.AND.Y.LT.1.2)I1=300
      DO 5 I=1,I1
      IF(Y.GT.-1.2.AND.Y.LT.1.2)GO TO 7
      Z=.025*I-.025
      GO TO 10
    7 Z=.010*I-.010
   10 Z=F*Z
      IF(Y.EQ.0.0.AND.Z.EQ.0.0)GO TO 5
      IF(((Y+1)*(Y+1)+Z*Z).LT.1)GO TO 5
      IF(((Y-1)*(Y-1)+Z*Z).LT.1)GO TO 5
      R=SQRT(Y*Y+Z*Z)
      DP=PI*Z/R/R
      IF(ABS(DP).GT.150)GO TO 5
      A1=COSH(PI*Z/R/R)-COS(PI*Y/R/R)
      IF(ABS(A1).LT.0.0001)GO TO 5
      A2=SINH(PI*Z/R/R)/A1
      IF(ABS(A2).LT.0.001)GO TO 5
      A3=0.0-SIN(PI*Y/R/R)/A1
      IF(ABS(A3).LT.0.001)GO TO 5
      A4=SQRT(A2*A2+A3*A3)
      IF(A4.EQ.0.0)GO TO 5
      PSI=ALOG(A4)
      IF(PSI.LE.0.)GO TO 5
      IF (PSI.LT.PSIL)GO TO 5
```

```
      IF (PSI.LT.PSIU.AND.PSI.GT.PSIL)GO TO 45
      GO TO 5
   45 N1=N1+1
      N2(J)=N2(J)+1
      IF(N2(J).GE.2)GO TO 2
      G(N1)=Z+5.0
      H(N1)=Y+5.5
      GO TO 5
    2 N1=N1-1
    5 CONTINUE
    4 CONTINUE
      CALL LINE(G,H,N1,+1)
    9 CONTINUE
   15 CONTINUE
      CALL PLOT(0.,0.,-4)
      STOP
      END
```

REFERENCES

Allen, H. Julian and Perkins, Edward W., A Study of Effects of Viscosity on Flow Over Slender Inclined Bodies of Revolution , NACA Technical Report Number 1048, 1951.

Bar-Lev, M., and Yang, H. T., "Initial Flow Field over an Impulsively Started Circular Cylinder", Journal of Fluid Mechanics, Vol. 72, Part 4, Pgs. 625-648, December, 1975.

Carrier, G. F., Krook, M., and Pearson, C. E., Functions of a Complex Variable; Theory and Technique , New York, McGraw Hill, 1966.

Glaister, D. H., Editor, "Biodynamic Response to Windblast", AGARD Conference Proceedings Number 170, July, 1975.

Gradshteyn, I. S., and Ryzhik, I. M., Table of Integrals, Series, and Products , New York, Academic Press, 1965.

Horner, T. W., and Hawker, F. W., A Statistical Study of Grip Retention Force , Aerospace Medical Research Laboratory, Technical Report No. AMRL-TR-72-110 (AD 767904), May 1973.

Marshall, F. J., and Deffenbaugh, F. D., "Separated Flow Over a Body of Revolution", Journal of Aircraft, Vol. 12, No. 2, Pgs. 78-85, February, 1975.

Mello, J. F., "Investigation of Normal Force Distributions and Wake Vortex Characteristics of Bodies of Revolution at Supersonic Speeds", Journal of the Aerospace Sciences, Vol. 26, No. 3, Pgs. 155-168, March, 1959.

Payne, P. R., "On Pushing Back the Frontiers of Flail Injury", in: Glaister, D. H., Editor, Biodynamic Response to Windblast, AGARD Conference Proceedings Number 170, Pages B9-1 - B9-7, July, 1975.

Payne, P. R., Hawker, F. W., and Euler, A. J., Extended Measurements of Aerodynamic Stability and Limb Dislodgement Forces with the ACES II Ejection Seat , Aerospace Medical Research Laboratory Report No. AMRL-TR-75-15 (AD A-044217), July 1975.

Sarpkaya, T., "An Analytical Study of Separated Flow About Circular Cylinders", ASME Paper Number 68-FE-15, Transactions of the American Society of Mechanical Ergineers, Journal of Basic Engineering, 1968.

Schneck, D. J., "Aerodynamic Forces Exerted on an Articulated Body Subjected to Windblast", Aerospace Medical Research Laboratory Report No. AMRL-TR-76-109, December, 1976.

Shames, Irving H., Mechanics of Fluids , New York, McGraw-Hill Book Company, Inc., 1962.

☆U.S.Government Printing Office: 1979 — 657-002/396